Far-infrared analysis of $In_{1-x}Ga_xSb$ films grown on GaAs by metal-organic magnetron sputtering

M. Macler, Z. C. Feng, and S. Perkowitz
Department of Physics, Emory University, Atlanta, Georgia 30322

R. Rousina and J. Webb
Institute for Microstructural Science, National Research Council Canada, Ottawa, Ontario, Canada K1A OR6
(Received 6 January 1992)

Infrared reflectivity spectra over 50–450 cm^{-1} yield phonon, band, and transport information for $In_{1-x}Ga_xSb$ films grown on GaAs by metal-organic magnetron sputtering. The infrared effective masses for *n*-type samples with $x=0$ and 0.01 agree with theory and with other measurements. The infrared masses for *p*-type material agree with theory at lower carrier densities, and increase with carrier concentration. The dependence of the longitudinal- and transverse-optical (TO) phonon mode frequencies on the alloy parameter x is given. The TO frequencies are higher than in bulk $In_{1-x}Ga_xSb$ for the InSb-like modes, possibly due to strain arising from the lattice mismatch between the film and the substrate. For most of the films, the thickness and resistivity derived from the infrared data agree well with values from scanning electron microscopy and van der Pauw resistivity measurements, respectively.

I. INTRODUCTION

The III-V semiconducting alloy $In_{1-x}Ga_xSb$ has, since 1970, been identified as a promising material for infrared detectors.[1] As modern applications require integrated optoelectronic devices, it is necessary to grow $In_{1-x}Ga_xSb$ in microstructure on materials appropriate for such devices, such as Si and GaAs. Recently, the technique of metal-organic magnetron sputtering (MOMS) has successfully deposited epitaxial layers of $In_{1-x}Ga_xSb$ on GaAs substrates over the entire compositional range.[2,3] These films have been characterized by surface morphology, x-ray diffraction, electron micrography, secondary-ion-mass spectrometry, Hall measurements, optical absorption, Raman scattering, and near-infrared spectroscopy.[2–4]

Here we extend our previously reported[4] far-infrared (FIR) and Raman analyses of $In_{1-x}Ga_xSb$ films grown on high-resistivity (100) GaAs to include four additional sample compositions. One aim is to better understand the fundamental properties of this relatively unexplored III–V ternary. We measure and report the transverse- and longitudinal-optical mode frequencies at 80 and 300 K over the entire range of x, to our knowledge the first such work since the measurements of Brodsky *et al.*[5] in 1970, and the first report for thin $In_{1-x}Ga_xSb$ films. We also present measured values for electron and hole masses and compare them to calculations, a contribution to the band theory of this alloy. A second broad aim is to illustrate the ability of infrared methods to characterize heterostructures. We compare film thicknesses and resistivity derived from our infrared measurements to those obtained by more conventional means, and find good agreement.

II. SAMPLES AND EXPERIMENTAL METHODS

The $In_{1-x}Ga_xSb$ films were deposited on semi-insulating GaAs substrates ($\rho=2\times10^7$ Ω cm) by MOMS at the National Research Council (NRC) Canada. An Sb target was sputtered in a reactive gaseous mixture of $In(CH_3)_3$ and $Ga(CH_3)_3$, with the gas mixture injected just above the heated substrate, to form In and Ga by thermal decomposition of the precursors. The process also forms various hydrocarbons through methyl radical reactions. Most of these products are readily evacuated, but—as the C-Ga bond is fairly strong in $Ga(CH_3)_3$—some carbon atoms remain trapped in the film during growth, constituting the main source of impurities. Films containing more than 1% Ga were *p* type. Typically, increasing the Ga concentration decreased the resistivity. Further details are given in Ref. 2.

Films were made with $x=0$, 0.01, 0.035, 0.07, 0.24, 0.28, 0.32, 0.36, 0.56, 0.68, and 1, as determined by x-ray diffraction and energy-dispersive x-ray analysis. The film thicknesses, from 0.4 to 2.4 μm, were determined from scanning electron microscope (SEM) images. Hall and resistivity data, obtained in the van der Pauw geometry, showed that all samples were *p* type except for Sample No. 1 ($x=0$) and Sample No. 2 ($x=0.01$), and gave resistivities of 0.003–0.03 Ω cm. The film parameters are listed in Table I.

Infrared reflectivity measurements were made at Emory University. Spectra were recorded at sample temperatures of 80 and 300 K using a Grubb-Parsons Mark II cube interferometer.[6,7] A polished coin-silver mirror provided a reference for reflection measurements over the range 50–450 cm^{-1} at 4-cm^{-1} resolution. The incoming radiation encountered the sample surface at near-normal incidence. For each sample, several spectra were averaged to enhance the signal-to-noise ratio.

Raman-scattering experiments were also performed at Emory.[8,9] The samples, held at 80 K, were mounted in a near-backscattering geometry and were excited by an Ar^+ laser. The scattered light was dispersed by a triple spectrometer and detected by a sensitive optical multichannel analyzer at a resolution of 2–3 cm^{-1}. The Ra-

TABLE I. Growth parameters, electrical characteristics, and effective masses for MOMS-grown $In_{1-x}Ga_xSb$ films on GaAs substrates. The film thickness d is determined from SEM photographs. The carrier concentration N and mobility μ are the room-temperature values determined by van der Pauw measurements. The effective masses m^*/m_0 are determined by infrared analysis at room temperature.

Sample no.	Type	x	d (μm)	N (10^{18} cm^{-3})	μ (cm^2/V s)	m^*/m_0
1	n	0	1.69	0.2	1700	0.023
2	n	0.01	2.35	0.94	1550	0.036
3	p	0.035	1.6	1.7	121	
4	p	0.07	1.5	1.3	166	
5	p	0.24	1.94	10	49	
6	p	0.28	1.8	2.9	76	
7	p	0.32	1.8	2.3	84	
8	p	0.36	2.35	8.3	86	0.31
9	p	0.56	1.4	17	61	0.42
10	p	0.68	1.6	19	54	0.44
11	p	1	0.43	16	28	

man data provided longitudinal-optical (LO) frequencies and corroborated the transverse-optical (TO) mode frequencies from the infrared measurements.

III. THEORY AND ANALYSIS

Figure 1 shows a typical measured reflectivity spectrum with a theoretical fit. As in all the spectra, the region 50–150 cm^{-1} is dominated by free carriers and the region 150–350 cm^{-1} is dominated by lattice modes. The theoretical curve is derived from the classical multioscillator model for the lattice modes, and the Drude model for the free carriers.[6,7] These give the dielectric function $\varepsilon(\omega)$ and the complex refractive index $n+ik$

$$\varepsilon(\omega)=(n+ik)^2=\varepsilon_\infty+\sum_j \frac{S_j\omega_{Tj}^2}{(\omega_{Tj}^2-\omega^2-i\Gamma_j\omega)} - \frac{\omega_p^2\tau}{\omega\left[\omega+\frac{i}{\tau}\right]}, \quad (1)$$

where ω is the frequency; ε_∞ is the high-frequency dielectric constant; S_j, ω_{Tj}, and Γ_j are the oscillator strength, the transverse optical-phonon frequency, and the damping constant of the jth lattice oscillator, respectively; and ω_p and τ are the free-carrier plasma frequency and scattering time, respectively. The free-carrier concentration N, effective mass m^*, and mobility μ are related to ω_p and τ by $\omega_p^2=4\pi Ne^2/m^*$ and $\mu=e\tau/m^*$.

The theoretical reflectivity of the film-substrate combination was calculated using the refractive index from Eq. (1). A computer program[10,11] evaluated standard expressions for the reflectivity at the vacuum-film, film-substrate, and substrate-vacuum interfaces, all assumed to be abrupt, and calculated the reflection coefficient for the entire structure. The program varied the phonon and free-carrier parameters to obtain the best fit to the data, defined as that which minimized chi square. For the free carriers, this yielded ω_p and τ. From their definitions, this means that if m^* is known, the fit gives N and μ; or conversely, if N is known from an independent determination like a Hall measurement, m^* can be found. Even if m^* is not known, the FIR fit gives the dc resistivity

$$\rho=1/Ne\mu=4\pi/\omega_p^2\tau ,$$

which is independent of m^*. The fitting program also included interference effects. Since these depend on film thickness, the fits yielded this parameter as well. The spacing of the interference fringes generated in the film is about 0.5 cm^{-1}. Since the spectral resolution was coarser than this, the program carried out appropriate averages over the fringes.

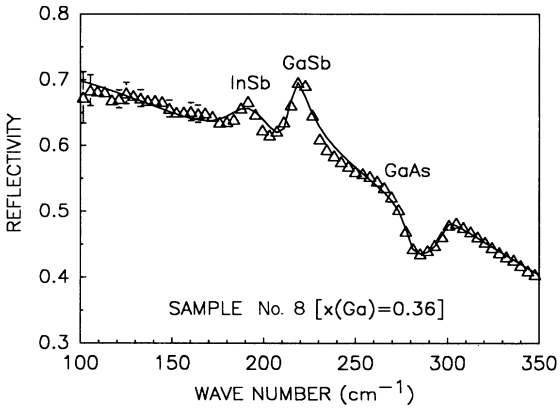

FIG. 1. Typical room-temperature FIR reflectivity spectrum for $In_{1-x}Ga_xSb$ film Sample No. 8 ($x=0.36$) grown on GaAs by MOMS. The triangles are experimental points. The solid line is the best fit derived from Eq. (1). Peaks corresponding to the InSb-like and GaSb-like TO modes in the film, and to the GaAs TO mode in the substrate, are marked.

IV. RESULTS AND DISCUSSION

The typical quality of the fits for all 11 samples was like that in Fig. 1, except for sample Nos. 3, 4, and 7 where the fit was poor near the TO mode from the GaAs substrate. This suggests a problem at the film-substrate interface, perhaps due to Ga diffusion. The resistivities and film thicknesses derived for these three samples are excluded from our analysis.

A. Film characterization: thickness and resistivity

Figure 2 shows film thicknesses derived from our fits to the room-temperature FIR data, compared to the values derived from SEM pictures, for all samples except Nos. 3, 4, and 7. The plot shows that the differences between the two measurement methods are random, and the two sets of values agree within 7% on average, which is certainly comparable to the sum of the errors involved. The thickness as determined from the FIR fitting procedure carries a statistical uncertainty of ~5%, which is increased by the uncertainty associated with the assumption that the film-substrate interface is perfectly abrupt. The determination by SEM also carries the ambiguity of locating the interface on a photograph.

Figure 3 compares (at 300 K) the resistivities derived from the infrared data, to the resistivities measured at NRC by van der Pauw-type electrical measurements. The FIR and the electrical values agree within 24% on average. The films with the largest discrepancies—Sample Nos. 5, 6, and 11—do not display significantly worse fits to the FIR data than the others, so the differences are not artifacts of the infrared analysis. They more likely represent actual differences, which may arise from film inhomogeneity, since an infrared beam and an electrical current give different averages over the film geometry. Nevertheless, the resistivity measurements are not corrected for such sources of error as finite contact size, and carry errors of ~10%. Since the uncertainty in the infrared value of resistivity is also of this order, an average difference of 24% is reasonable.

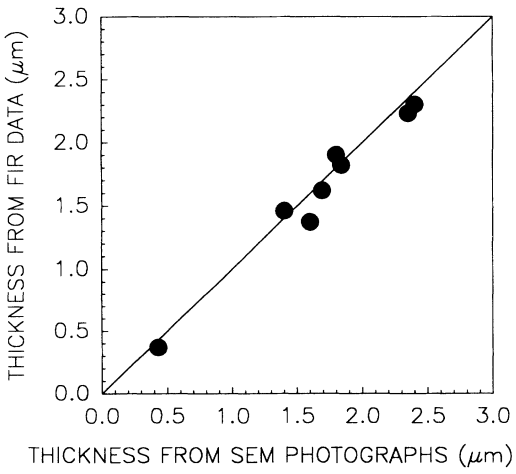

FIG. 2. Thickness of MOMS-grown $In_{1-x}Ga_xSb$ films on GaAs derived from infrared data at room temperature vs thickness from SEM images. The solid line represents perfect agreement between the two sets of results.

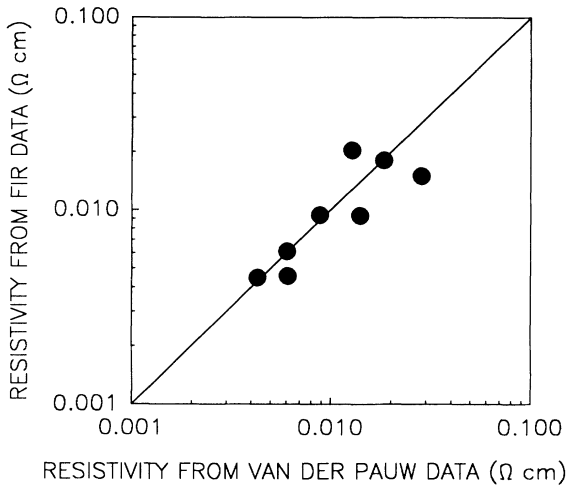

FIG. 3. Room-temperature resistivity for MOMS-grown $In_{1-x}Ga_xSb$ films on GaAs derived from infrared data vs resistivities from van der Pauw-type electrical measurements. The solid line represents perfect agreement between the two sets of results.

B. Fundamental properties: effective masses and phonon frequencies

We derived effective masses from those reflectivity spectra where the fit was good, and which gave values for film thickness and resistivity that agreed with the nominal values. The samples meeting these criteria were the two *n*-type film Sample Nos. 1 and 2, and the three *p*-type film Sample Nos. 8, 9, and 10. For these, we set N, μ, and the thickness at their nominal values, and varied m^* to give the best fit to the reflectivity data.

Of the two *n*-type samples, one is pure InSb and the other contains only 1% Ga. Hence, our results for m^*, given in Table I, can be compared to measured and calculated values in pure bulk InSb, which we do in Fig. 4. The theoretical dependence of m^* on carrier concentration comes from Kane's low-temperature model,[12,13] which yields the straight-line dependence of $[m^*/(1-m^*)]^2$ on $N^{2/3}$ shown in the figure. The value for Sample No. 1, our pure InSb sample with low carrier concentration, is in accord with theory and with other data. The result for Sample No. 2, with 1% Ga and a higher carrier concentration, is slightly higher than predicted by Kane's theory. Since m^* for GaSb exceeds that for InSb, this is expected. The good agreement between our m^* values and those from the literature validates our analysis.

For the *p*-type samples, interpretation of the hole effective-mass data is complicated by the fact that carrier concentration and alloy composition both vary from sample to sample. The variation in carrier concentration is a concern since the second valence band (VB_2) in InSb is not exactly parabolic in wave vector. Thus, the light-hole

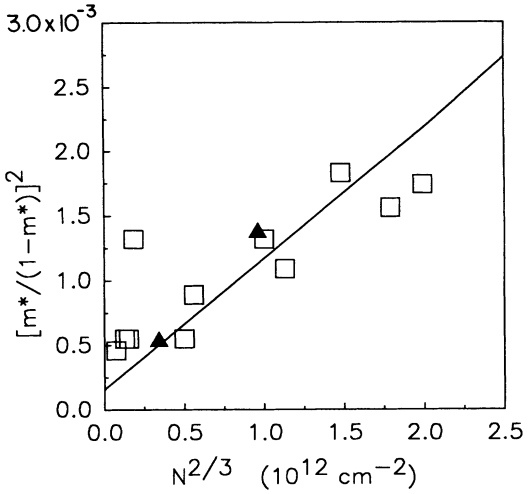

FIG. 4. $[m^*/(1-m^*)]^2$ vs $N^{2/3}$ for n-type bulk InSb and for MOMS-grown $In_{1-x}Ga_xSb$ on GaAs with $x=0$ and 0.01, where N is the carrier concentration and m^* is the carrier effective mass. The straight solid line is Kane's theoretical result. The open squares represent experimental results for bulk InSb from the literature [Ref. 13, and W. G. Spitzer and H. Y. Fan, Phys. Rev. **106**, 882 (1957)]. The solid triangles are the results from the present infrared work, which agree with theory and with the other measurements.

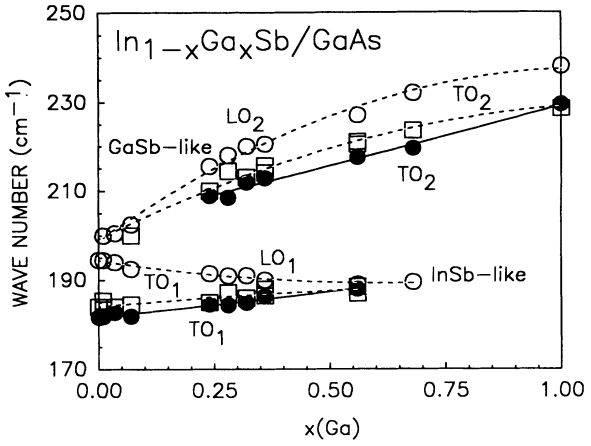

FIG. 5. TO and LO phonon mode frequencies vs x for MOMS-grown $In_{1-x}Ga_xSb$ on GaAs. Data at room temperature and at nitrogen temperature are represented by filled symbols and open symbols, respectively. Solid lines and dashed lines represent second-order regression fits to the room-temperature and nitrogen-temperature data, respectively. The TO mode frequencies are extracted from the fits to the infrared data with corroboration from Raman spectra, whereas the LO mode frequencies are extracted from Raman spectra.

mass should depend on carrier concentration, an effect expected to carry over to $In_{1-x}Ga_xSb$.

In bulk p-type $In_{1-x}Ga_xSb$, the compositional dependence of m^* has been unraveled by the use of piezoreflectance.[14] These data were analyzed within the framework of Kane's theory and effective masses were derived for heavy, light, and spin splitoff holes, throughout the alloy composition range. In optical measurements, only heavy and light holes are relevant. As the first (VB_1) and second (VB_2) valence bands are nearly degenerate at $\mathbf{k}=0$, the optical effective mass $m_{\rm opt}$ is given by the usual formula[15]

$$m_{\rm opt}=\frac{(m_1^{3/2}+m_2^{3/2})}{(m_1^{1/2}+m_2^{1/2})}\ , \tag{2}$$

where m_1 and m_2 are the heavy- and light-hole effective masses, respectively. We derived values of $m_{\rm opt}$ from Ref. 14, using Eq. (2). They showed no significant dependence on alloy composition over the whole range $x=0-1$, with a nearly constant value $m_{\rm opt}/m_0=0.3$ at low carrier concentration ($N=10^{16}-10^{17}$ cm^{-3}) and low temperature. Table I gives our measured results for $m_{\rm opt}$. The result $m_{\rm opt}/m_0=0.31$ for Sample No. 8, with $N=8.3\times10^{18}$ cm^{-3}, is very near the derived value. At the higher carrier concentrations in Sample Nos. 9 and 10, our measured $m_{\rm opt}$ increases significantly.

Our infrared spectra showed clear InSb-like TO modes for $x=0-0.56$, and GaSb-like modes for $x=0.24-1$, whereas the Raman spectra showed clear LO modes with evidence of TO modes as well. Figure 5 shows the compositional dependence of the TO and LO mode frequencies at 300 and 80 K. At 300 K, the TO mode frequencies are linear in x. When expressed in cm^{-1}, they are closely fitted by

$$\omega_{\rm TO}(\text{InSb-like})=181.7+11.2x,\quad 0\le x\le 0.56\ , \tag{3}$$

$$\omega_{\rm TO}(\text{GaSb-like})=202.4+26.7x,\quad 0.24\le x\le 1\ . \tag{4}$$

These equations provide a simple way to determine alloy composition from room-temperature FIR data. The uncertainty in x is larger at low x than at high, because the slope of the InSb-like mode frequency is smaller than that of the GaSb-like mode. At low values of x, its typical uncertainty is 0.1, dropping to 0.05 at higher values.

Our measured frequencies at 300 K for the GaSb-like TO modes in the films are almost identical to those[5] in bulk $In_{1-x}Ga_xSb$, but the frequencies of the InSb-like TO modes are shifted above the corresponding bulk values by 4 cm^{-1} on average. This systematic difference is significant compared to the measurement uncertainties. In the earlier work, the bulk samples of $In_{1-x}Ga_xSb$ were examined by optical and x-ray methods, to establish their homogeneity and composition, and spectra were measured to a resolution of 1–2 cm^{-1}. The TO frequencies were extracted from each spectrum by both Kramers-Kronig analysis and Lorentzian analysis, which returned the same frequencies to within 1 cm^{-1}. The only possible caveat may be that these early spectra were obtained with a grating spectrometer, whereas our work uses a Fourier spectrometer, which is superior in the far infrared. However, the earlier spectra appear to be of good quality.

The frequency shifts in the films may be due to a strain at the film-substrate interface, arising from the considerable difference in lattice constant between $In_{1-x}Ga_xSb$ and GaAs. The lattice constant of $In_{1-x}Ga_xSb$ exceeds

that of the GaAs substrate throughout the compositional range (the difference is 14% at $x=0$, and 9% at $x=1$), which should produce compressional strain in the film. However, it is not obvious why the InSb-like modes are shifted by this effect whereas the GaSb-like modes are not. The frequencies for both TO modes increase with decreasing temperature, which is not surprising. What is more intriguing is that the GaSb-like mode frequencies vs x show substantial curvature at 80 K, but not at 300 K. This is based on least-squares polynomial fits, which allowed for a quadratic term; as Fig. 5 shows, this term turned out to be significant at 80 K, and unnecessary at 300 K. It is possible that if more data points were available at 300 K for $x<0.24$, the curve at the higher temperature would also show some quadratic bowing. The InSb-like modes present little curvature at either temperature.

V. CONCLUSIONS

Infrared reflectivity data have yielded fundamental information about effective mass in *n*- and *p*-type $In_{1-x}Ga_xSb$ films grown on GaAs substrates by the MOMS method, and have also given reliable characterization data, layer thickness, and resistivity. Because this characterization information is obtained nondestructively, the infrared method has particular value compared to some other techniques. In combination with Raman data, the FIR data also yield a complete picture of the alloy's TO- and LO-phonon mode frequencies. One interesting feature in the films is the fact that the InSb-like mode is shifted, but the GaSb-like mode is not, relative to the only existing set of results[5] for bulk $In_{1-x}Ga_xSb$. (It would, of course, be valuable to repeat these early measurements using Fourier spectroscopy.) These shifts may be related to the selective effects of stress due to the film-substrate lattice mismatch. The differences in shape of the mode frequency versus x curves may also be worth further attention; in any case, the simple linear dependence at 300 K of TO frequencies on x provides another useful characterization tool for the system. We will continue to investigate the temperature dependence of the TO-phonon mode frequencies, together with the effects of strain on these phonons.

Perhaps the most important general conclusion is to note the wealth of information about film $In_{1-x}Ga_xSb$ that comes from careful analysis of the FIR spectra. The combination of fundamental and characterization information that can be extracted from a measurement of a reflectivity spectrum is probably unmatched by any other common semiconductor probe. These latest results for $In_{1-x}Ga_xSb$ on GaAs strengthen the already great capability[16] of infrared analysis to probe both established and novel semiconductor systems and microstructures, as we have shown in other III–V and II–VI systems.

[1]C. Hilsum, Electron. Lett. **6**, 448 (1970).
[2]R. Rousina, J. B. Webb, and J. P. Noad, in *Layered Structures: Heteroepitaxy, Superlattices, Strain, and Metastability,* edited by B. W. Dodson, L. J. Schowalter, J. E. Cunningham, and F. H. Pollak, MRS Symposia Proceedings No. 160 (Materials Research Society, Pittsburgh, 1990), p. 427.
[3]R. Rousina, C. Halpin, and J. B. Webb, J. Appl. Phys. **68**, 2181 (1990).
[4]Z. C. Feng, S. Perkowitz, R. Rousina, and J. B. Webb, Can. J. Phys. **69**, 386 (1991).
[5]M H. Brodsky, G. Lucovsky, M. F. Chen, and T. S. Plaskett, Phys. Rev. B **2**, 3303 (1970).
[6]S. Perkowitz and J. Breecher, Infrared Phys. **13**, 312 (1973).
[7]S. Perkowitz and R. H. Thorland, Phys. Rev. B **9**, 545 (1974).
[8]Z. C. Feng, S. Perkowitz, T. S. Rao, and J. B. Webb (Ref. 2), p. 739.
[9]Z. C. Feng, S. Perkowitz, T. S. Rao, and J. B. Webb, J. Appl. Phys. **68**, 5363 (1990).
[10]T. W. Cadman and D. Sadowski, Appl. Opt. **17**, 531 (1978).
[11]C. E. Jones, M. E. Boyd, W. H. Konkel, S. Perkowitz, and R. Braunstein, J. Vac. Sci. Technol. A **4**, 2056 (1986).
[12]O. Madelung, *Physics of III-V Compounds* (Wiley, New York, 1964), p. 95.
[13]E. D. Palik and G. B. Wright, in *Semiconductors and Semimetals, Vol. 3,* edited by R. K. Willardson and A. C. Beer (Academic, New York, 1967), pp. 456–457.
[14]D. Auvergne, J. Camassel, H. Mathieu, and A. Joullie, J. Phys. Chem. Solids **35**, 133 (1974).
[15]H. Y. Fan (Ref. 13), pp. 414–415.
[16]S. Perkowitz, in *Infrared and Millimeter Waves,* edited by K. J. Button (Academic, New York, 1983), Vol. 8, pp. 71–125.